Directional strengthening and weakening in hydrodynamically sheared granular beds

Marios Galanis, Mark D. Shattuck, Corey S. O'Hern, and Nicholas T. Ouellette

Phys. Rev. Fluids **7**, 013802 — Published 21 January 2022

DOI: 10.1103/PhysRevFluids.7.013802

Directional strengthening and weakening in hydrodynamically sheared granular beds

Marios Galanis,[1] Mark D. Shattuck,[2] Corey S. O'Hern,[3,4,5] and Nicholas T. Ouellette[1,*]

[1]*Department of Civil and Environmental Engineering, Stanford University, Stanford, California 94305, USA*

[2]*Benjamin Levich Institute and Physics Department, The City College of the City University of New York, New York, New York 10031, USA*

[3]*Department of Mechanical Engineering and Materials Science, Yale University, New Haven, Connecticut 06520, USA*

[4]*Department of Applied Physics, Yale University, New Haven, Connecticut 06520, USA*

[5]*Department of Physics, Yale University, New Haven, Connecticut 06520, USA*

Abstract

Granular beds driven by overlying shear flows begin to erode when the stress delivered to the bed by the fluid exceeds a critical value. Previous studies have shown that this critical stress depends on the stress history of the bed, and that beds will strengthen when subjected to subcritical stresses. By measuring the behavior of erodible beds in a laboratory flume, we confirm this strengthening effect, but also find that it is strongly directional. We find that preconditioned granular beds are indeed more resistant to erosion when driven in the direction of the conditioning flow, but that this strengthening is accompanied by a weakening when driven in other directions. Preconditioned beds are in fact more susceptible to erosion by flows in the direction opposite to that of the conditioning flow than freshly settled beds are. Our results show that the strength of a natural erodible bed with a stress history is likely to be highly anisotropic, with significant implications for predictions of sediment transport.

I. INTRODUCTION

Much of the surface of the earth is composed of granular materials [1], which are always in contact with fluids (primarily water and air). When these fluids flow, the stresses they impart can dislodge and remove grains, leading to erosion and weathering [2]. The susceptibility of a granular bed to erosion by a given flow is typically evaluated by computing the Shields number Θ, which compares the shear stress at the granular bed to the weight of an individual grain. Classically, it is assumed that once the Shields number exceeds a critical value (that depends additionally on the particle Reynolds number), grains will be mobilized from the bed into bedload transport [3, 4]. However, it is widely acknowledged that this framework is oversimplified [1, 5].

One reason why the classical Shields framework does not perform well is that it incorporates little of the nuance of the physics of granular materials [6, 7]. Of particular relevance to the experiments we discuss here, driven granular materials are well known to contain an imprint of their stress history [8]. As the material evolves, some of the grain-grain contacts are loaded preferentially over others, and the material develops line-like structures known as force chains that carry most of the internal stress and stabilize the material against further

* nto@stanford.edu

deformation [9, 10]. Force chains do not develop isotropically; rather, their structure and directionality are reflective of the stresses applied to the material [11]. For this reason, even though granular materials may strengthen over time when subjected to stresses applied in the same direction, they may at the same time weaken against stresses applied in a different direction [12–16].

A similar mechanism may also exist in hydrodynamically driven geophysical granular materials. Natural riverbeds, for example, can exhibit strengthening behavior as they evolve. The most well known mechanism for this strengthening is the phenomenon known as armoring. Riverbed armoring is typically understood to describe grading processes leading to larger particles appearing on the surface, driven by, for example, preferential erosion of smaller particles or preferential deposition of heavier, larger entrained particles [17, 18]. However, granular mechanics can also play a role in bed strengthening. It has been recognized in field observations, for example, that the amount of sediment transport by a particular flood event is dependent on the strength of prior events, suggesting that the stress history of the bed is an important parameter [19–21]. Laboratory measurements have confirmed that the stress history of a subcritically driven bed can modify the subsequent critical stress required to mobilize it [22–26], and have suggested some explanations for this phenomenon such as compaction [22] or smoothing and rearrangement of the bed surface [25, 26]. The similarity between the observation of history dependence in these geophysical examples and in the granular physics community suggest the possibility of associated weakening in hydrodynamically driven granular materials when the bed is driven in a direction different from the original flow. This situation may not be likely in steep rivers and streams, but may occur in sporadically in coastal environments during, for example, storms or regularly in tidal systems.

To investigate this question of whether bed strengthening is associated with concomitant weakening in directions different from the original flow, we carried out experiments in a closed laboratory flume containing an erodible granular bed. We pre-conditioned the bed by subjecting it to a turbulent shear flow delivering nominally subcritical stresses, and then compared the onset of grain motion when it was driven in the prior flow direction or opposite to it. We find that, as expected, the onset of grain motion occurs at higher Shields number (so that erosion is suppressed) when the bed is driven in the same direction as the conditioning flow, but that it occurs at lower Shields number (so that erosion is enhanced) when driven in

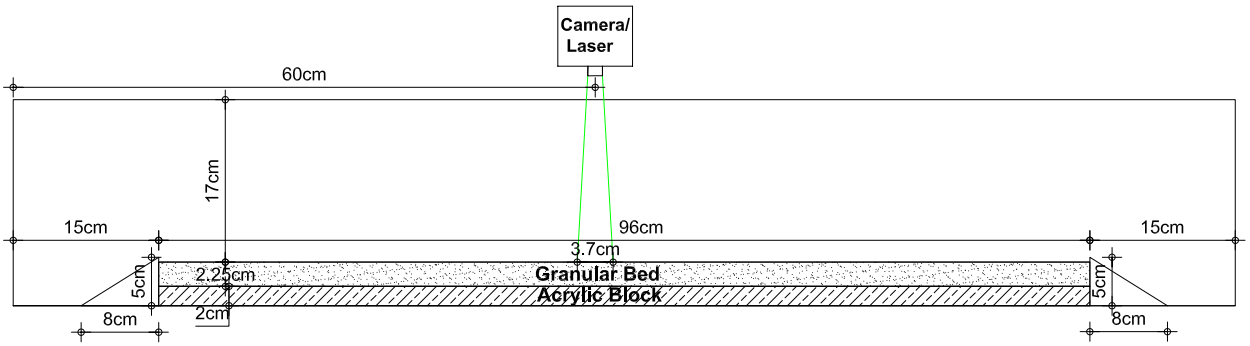

FIG. 1. Diagram of the test section of the apparatus. The measurement region is indicated by the position of the overhead camera (for measurements of the grain motion) or laser (for measurements of the flow).

the opposite direction. Indeed, mobilization of a pre-stressed bed by oppositely directed flows is easier than mobilization of a freshly settled bed. Additionally, we find that the sediment flux is larger at a given Shields number above the onset of motion when the bed is driven in the opposite direction than when it is driven in the same direction as the conditioning flow. This enhancement is primarily due to an increase in the number of mobilized grains, though to a lesser extent we also find that mobilized grains have higher velocities when driven in the opposite direction. Our findings support the notion that bed strengthening has a component that arises from changes in the granular force and contact networks and thus is directional—and that strengthening is thus likely to be typically accompanied by weakening. These results in turn imply that erosion due to flows moving in unusual directions (such as during storms) may be more severe than would be predicted in a typical Shields framework, and also suggest strategies for enhancing the mobilization of natural sediment beds.

We begin in Sec. II by describing our apparatus and experimental protocols. In Sec. III, we then present our results, including measurements of the mean grain velocities and a more detailed statistical analysis. Finally, in Sec. IV, we summarize our findings and discuss their implications.

II. METHODS

A. Apparatus

Our experimental apparatus consists of two straight sections joined by U-shaped bends. It is a closed channel with a width of 5.08 cm and a height of 21.25 cm. The flow in the channel is similar to a plane Couette flow. It is driven by a toothed belt connected to an external motor mounted at the top of the apparatus in the middle of one of the straight sections. The driving belt is completely immersed in water, and the entire apparatus is sealed (without any free surface), so that air is not entrained into the water. The bulk flow velocity is set by controlling the motor speed and is measured using detailed velocimetry conducted after every experiment, as described below. The other straight section is the test section where the measurements are taken, and is sketched in Fig. 1. The test section is constructed with glass sidewalls and an acrylic top plate for optical access, so that both the fluid flow and the granular bed can be imaged. The granular bed is placed in the test section and is constrained by two triangular wedges 5 cm in height and fixed to the channel floor. The two wedges prevent large-scale migration of the bed, keeping most of the grains in the test section and delaying the formation of large-scale bedforms. At higher flow rates, there can be some flow separation from the top of these wedges; our measurement region is far enough downstream, however, that this separation does not affect our measurements. Below the granular bed we have inserted an acrylic plate of 2 cm height, to reduce the total amount of granular material required in each experimental run. Even with this spacer, the granular bed is deep enough so that the bottom boundary condition does not affect the fluid-grain interface.

B. Flow characterization

To obtain an accurate measurement of the fluid flow, we used particle tracking velocimetry (PTV). We seeded the fluid with neutrally buoyant fluorescent polyethylene microspheres with a diameter of approximately 50 μm that acted as tracer particles. We aimed a vertical laser sheet through the centerline of the test section, with the thin direction of the sheet in the spanwise direction. The motion of the microspheres was imaged with a 1-megapixel Photron Fastcam SA5 camera looking through the sidewall of the channel at a constant frame

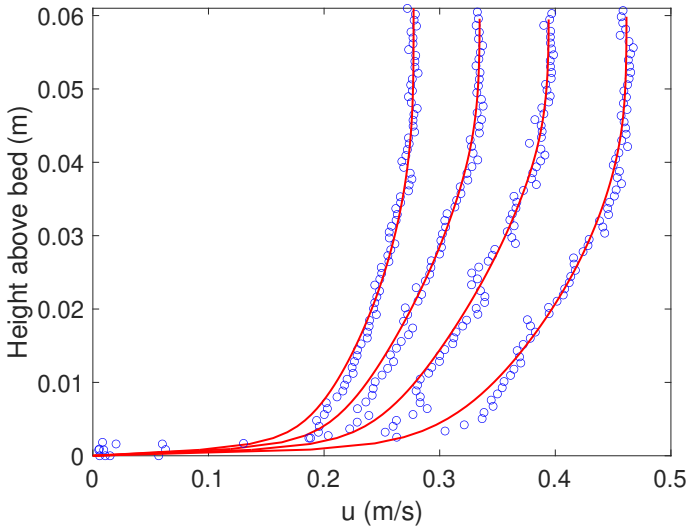

FIG. 2. Example velocity profiles measured for freshly settled beds for four different flow speeds. The solid curves are fits to the particle-tracking data (see text for details).

rate of 1000 frames per second, so that the time between images was 1 ms. We recorded multiple brief 5 s videos of the moving tracers, and reconstructed their motion using a predictive multiframe tracking algorithm [27]. Using the particle trajectories, we computed accurate velocities via convolution with a smoothing and differentiating kernel [28]. Because we could not directly control the flow velocity, we performed PTV measurements for each experimental run. We conducted the PTV with the sediment bed present to ensure that the flow properties were measured in the presence of the appropriate boundary conditions in the experimental runs. We limited the flow speeds to those below or just above the onset of sediment motion and only measured the flow within a thin light sheet in the center of the channel; thus, the number of moving sediment grains observed during PTV was statistically negligible compared to the number of tracer particles. To estimate the hydrodynamic stress applied to the granular bed, we used the PTV measurements to reconstruct a well-resolved vertical velocity profile. We first binned the measured velocities of tracer particles based on their vertical position into bins 2 mm in height, ensuring that each bin contained at least 20 000 samples. Subsequently, we fit the velocity profile using the method described by Rodríguez-López *et al.* [29], who give a functional form for the profile and a scheme for robustly fitting its parameters. This method allowed us to extract the wall shear stress τ_w and the friction velocity $u_* = \sqrt{\tau_w/\rho_f}$, where ρ_f is the density of water. Examples of the

measured velocity profiles and fits are shown in Fig. 2 for four different flow rates; we note that there was no significant spanwise variation in the velocity profile, aside from very close to the channel side walls. After calculating τ_w, we computed the Shields number for our grains as

$$\Theta = \frac{\tau_w}{(\rho_g - \rho_f)gD}, \tag{1}$$

where ρ_g is the grain density, g is the acceleration due to gravity, and D is the grain diameter. In our experiments, the friction Reynolds number $Re_t = u_*\delta/\nu$, where δ is the half-height of the channel in the test section and ν is the kinematic viscosity of water, ranges from 900 to 1925, and the shear Reynolds number at the grain scale $Re_* = u_*D/\nu$ ranges from 5.3 to 11.3.

C. Granular bed

The erodible bed was composed of soda lime glass beads with a mass density of $\rho_g = 2.5$ g/cm^3 that were sieved so that their diameter lies in the range of $D = 0.625 \pm 0.125$ mm. We used grains of only one nominal size rather than a mixture of grains of different sizes so that we can distinguish armoring via grading processes from strengthening due to granular mechanics. The bed was imaged with a FLIR Grasshopper 3 color camera mounted above the apparatus looking vertically down through the acrylic top plate. Images measuring 992×920 pixels with a spatial resolution of $37\mu m$ per pixel were captured at a rate of 100 frames per second. We placed the camera in the middle of the test section, far from the U-shaped turn, so that secondary flows from the bend and the beginning of the granular bed will have decayed before reaching the measurement area. To track the motion of individual grains we used the same algorithms described in Ref. [7]. To make the detection of individual grains easier and more reliable [30–32], we used two colors of grains (blue and gold) in an 88/12 mixture by volume, and only identified the gold grains (which only occupied 12% of the volume). To locate the gold grains, as explained in Ref. [7], we first transformed the red-green-blue (RGB) images produced by the camera into the hue-saturation-value (HSV) color space. We then segmented the images into pixels belonging to blue grains and pixels belonging to gold grains using a standard k-means clustering algorithm (with $k = 2$) on the H component of the images. Finally, we identified individual gold grains using a circular Hough transform.

D. Experimental protocol

Before each experimental run, the erodible bed was prepared by mixing the two colors of grains in a container and then pouring them through a funnel into the test section of the channel. We moved the funnel along the test section as we added the grains so that the depth was roughly uniform, and then gently smoothed the bed to make its top surface flat. The weight of added grains was kept fixed from experiment to experiment, and produced a granular bed roughly 2.25 cm deep. The apparatus was then filled with water. For all but one of our experimental cases, we next subjected the bed to a subcritical stress—that is, to a flow with a Shields number below the nominal critical value above which bedload transport occurs, and where additionally we did not visually observe any grains moving. For the experiments reported here, we used a Shields number of $\Theta = 0.013$ (approximately 80% of the critical stress for a freshly settled bed) for the bed conditioning. We applied this conditioning flow for four different durations: 360 s, 776 s, 1671 s, and 3600 s. We then stopped the motor and allowed the fluid to come to rest completely.

After conditioning, we followed a protocol similar to what we have done previously [7, 32] to study the onset of grain motion with the bed driven in either the same direction as the conditioning flow or in the opposite direction. Starting with a flow in the desired direction with a subcritical Shields number, we increased the flow velocity quasistatically in small increments of approximately 6 cm/s. After each increase, the system was allowed to stabilize for 15 s, after which a movie of the bed was captured. To avoid contamination of our results by the development of bedforms for flow cases above the onset of grain motion, we limited the duration of these movies to 40 s, since we observed empirically that bedforms take longer than this amount of time to develop and migrate into the measurement region. We also only considered flow speeds near the onset of bed motion, and did not approach the transition to suspended-load transport. We note that the bed was prepared independently before each experiment so that measurements of the onset of motion were always made on a freshly conditioned bed, regardless of the flow direction.

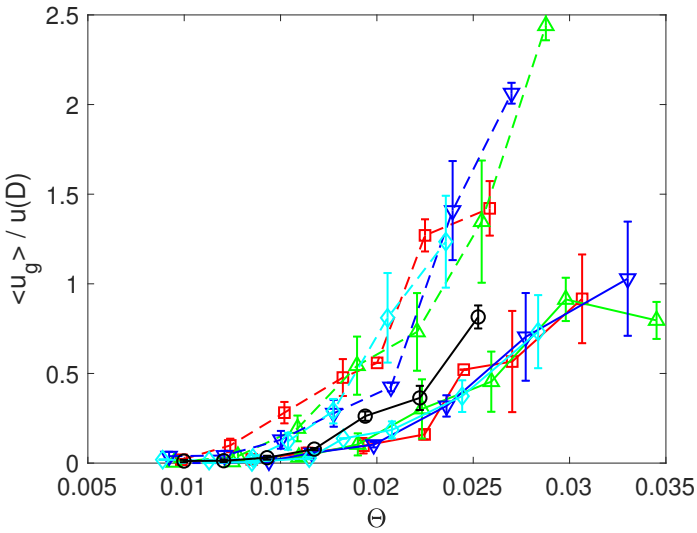

FIG. 3. Mean grain velocity $\langle u_g \rangle$ averaged over all identified grains as a function of Shields number Θ. The grain velocities are scaled by $u(D)$, the fluid velocity one grain diameter above the bed. Data are shown for several cases. Different symbols indicate different durations of the conditioning flow: 0 s (that is, freshly settled beds; black circles), 360 s (red squares), 776 s (green triangles), 1671 s (blue inverted triangles), and 3600 s (cyan diamonds). Solid lines indicate measurements made with the flow in the same direction as the conditioning flow, and dashed lines indicate that the flow was in the opposite direction. Error bars show the standard error computed over three trials.

III. RESULTS

A. Mean grain motion

We begin by considering the simplest metric for characterizing the onset of motion in an erodible bed: the mean grain velocity $\langle u_g \rangle$ as a function of the Shields number. This mean velocity is typically proportional to the downstream flux of grains [32], which is often used as an indicator for the onset of erosion [3, 30]. We computed $\langle u_g \rangle$ simply by averaging the measured velocity of each grain identified by our particle-tracking algorithm at each time step, whether it was exhibiting net downstream motion or not. Thus, $\langle u_g \rangle$ will in general be smaller than the typical velocity of a moving grain, since most of the bed grains remain stationary until the flow strength is well above the onset of motion.

Our measured values of $\langle u_g \rangle$ as a function of the Shields number Θ are shown in Fig. 3, where we normalize $\langle u_g \rangle$ by $u(D)$, the mean streamwise flow velocity one grain diameter above the bed (taken from the measured velocity profile). We have shown previously that this value is an appropriate scaling variable for $\langle u_g \rangle$ [7], as it is the typical flow velocity that a grain in bedload transport will experience.

The data in Fig. 3 falls into three distinct groups. Measurements for freshly settled beds with no stress history fall on one onset curve. Although extracting critical Shields numbers is imprecise for beds driven by turbulent flows [32], the approximate value of the critical Shields number one can estimate from this data is consistent with what one would expect from a traditional Shields-curve analysis [3]. Once the bed has been subjected to a conditioning flow with subcritical stresses, however, its onset curve shifts and the critical Shields number increases: as one would expect, beds with stress history require more stress to mobilize. An implication of this result is that the critical Shields number for bed mobilization depends on more than just the flow state (as described by the Reynolds number), and that the granular microstructure also plays a role. We also find that the onset curve is insensitive to the duration of the conditioning flow, at least for the durations and subcritical stress magnitudes we tested. This behavior is different from what has been observed in large-scale geophysically motivated experiments [22–24], where bed strength was found to be enhanced for longer flow conditioning durations. However, results similar to ours were reported for erodible beds driven by laminar flows [33], where it was found that the critical stress was only strongly dependent on the conditioning duration when the subcritical stress was very close to the critical value.

Our measurements for the onset of motion of stressed beds driven in the direction opposite that of the conditioning flow fall into a third group. These cases are not only easier to mobilize than the strengthened beds driven in the same direction as the conditioning flow, but are in fact easier to mobilize than freshly settled beds. Thus, we find that strengthening a granular bed with a shear flow does in fact weaken it against stresses applied in other directions. As with the increase in strength after conditioning when driven in the conditioning direction, we find that this weakening is insensitive to the duration of the conditioning.

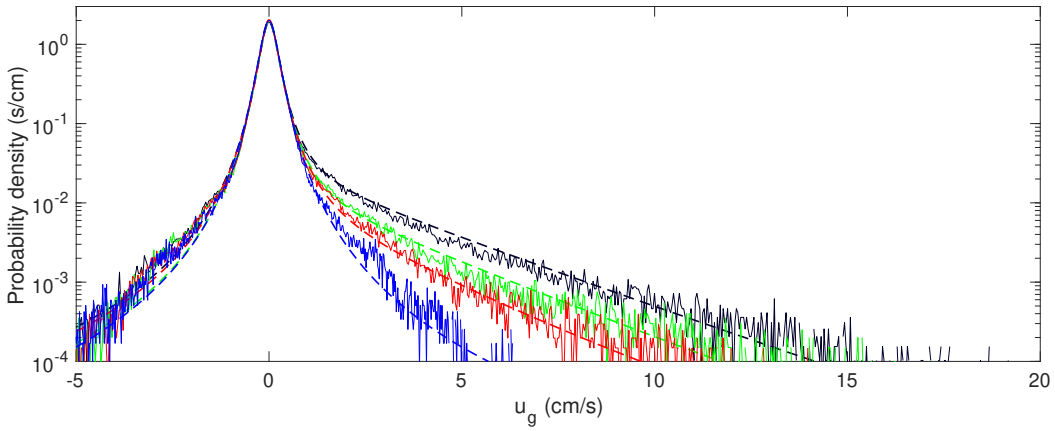

FIG. 4. Grain velocity PDFs for $\Theta = 0.012$ (blue), 0.019 (red), 0.022 (green), and 0.025 (black) for freshly settled beds. The dashed lines are fits to the mixture model described in the text.

B. Higher-order statistics

Because it is an average over the behavior of all identified grains, $\langle u_g \rangle$ can increase because the velocity of individual grains increases, because more grains are moving, or both. Simply placing a threshold on the grain velocity is not a reliable way to distinguish grains with net downstream velocity from those that are jittering in place without being entrained, since bed grains can respond to turbulent velocity fluctuations that are not necessarily small compared to the typical speed of grains entrained into bedload transport [32]. Thus, to gain a better understanding of the grain dynamics after exposing them to subcritical stresses, we turn to an analysis of the full probability density functions (PDFs) of the grain velocity.

In Fig. 4, we show the PDFs of the instantaneous grain velocity u_g measured in freshly settled beds for four different Shields numbers. For Shields numbers below the onset of net grain motion, the PDFs are symmetric about $u_g = 0$, indicating that the grains are simply moving slightly in place in response to the turbulent fluctuations but are not exhibiting sustained downstream motion. As the Shields number increases, however, the PDFs develop a long exponential tail that can be interpreted as evidence for stochastic and independent mobilization of individual grains into bedload transport [34, 35]. As we have done previously [7, 32], we fit these PDFs to a mixture model of a student's t-distribution, to capture the symmetric inner core and its heavier-than-Gaussian tails, and an exponential distribution.

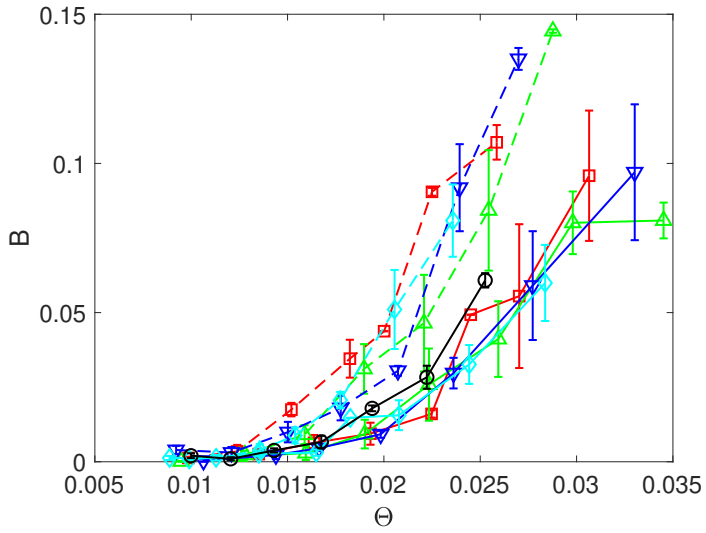

FIG. 5. The fraction of mobilized grains B as determined from fits to the mixture model in Eq. 2 as a function of the Shields number Θ. Symbols, line styles, and error bars have the same meanings as in Fig. 3.

The model is given by

$$P(u_g) = A\frac{\Gamma\left(\frac{\zeta+1}{2}\right)}{\sigma\sqrt{\zeta\pi}\Gamma\left(\frac{\zeta}{2}\right)}\left[\frac{\zeta+\left(\frac{u_g}{\sigma}\right)^2}{\zeta}\right]^{\left(-\frac{\zeta+1}{2}\right)} + BH(u_g)\frac{1}{u_g^*}e^{-u_g/u_g^*}, \tag{2}$$

where A and B are the relative weights of each distribution in the mixture (and where $A + B = 1$), σ sets the characteristic width of the t-distribution and is related to the magnitude of the typical velocity fluctuations, ζ controls the heaviness of the the t-distribution tails (with the distribution approaching a Gaussian as $\zeta \to \infty$), and u_g^* is the characteristic magnitude of the velocity of mobilized grains. Γ is the gamma function, and H is the Heaviside function (so that the exponential part of the model PDF is only included for positive u_g). We fit this model to our data using a standard nonlinear least-squares algorithm. Fits of this model to the measured PDFs are shown in Fig. 4 with dashed lines.

Here, we focus on the parameters B, which tells us the fraction of identified grains that are mobilized into bedload transport, and u_g^*, which gives us the typical velocity of these mobilized grains. These parameters give us direct information about the mobilized grains, while σ and ζ tell us more about the response of non-mobilized grains to the turbulent fluctuations. In Fig. 5, we show the measured values of B as a function of Shields number for the same cases as reported in Fig. 3: freshly settled beds, beds exposed to a subcritical stress

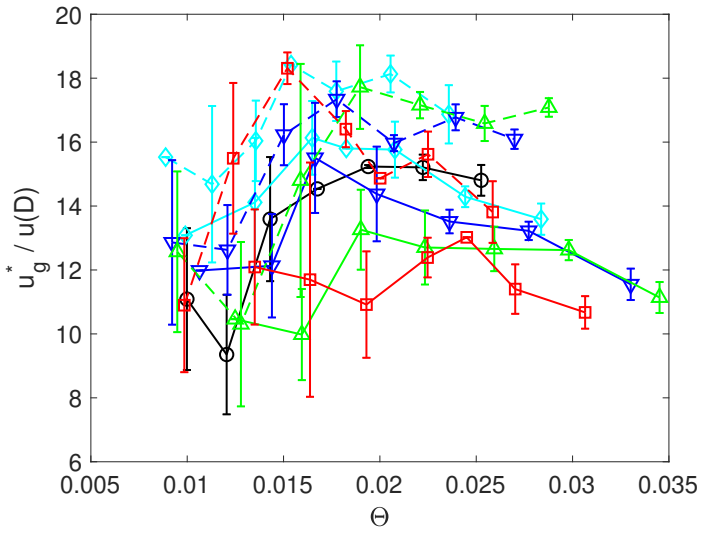

FIG. 6. The typical velocity of mobilized grains u_g^* as determined from fits to the mixture model in Eq. 2 as a function of the Shields number Θ. u_g^* is scaled by $u(D)$, the fluid velocity one grain diameter above the bed. Symbols, line styles, and error bars have the same meanings as in Fig. 3.

and driven in the same direction, and strengthened beds driven in the direction opposite the conditioning flow. The behavior of B as a function of Θ is largely similar to the behavior of $\langle u_g \rangle$. For the same value of Θ, fewer grains are entrained into bedload transport in conditioned beds driven in the conditioning direction as compared with freshly settled beds, but more grains are entrained when they are driven in the opposite direction. B is again insensitive to the duration of exposure to the conditioning flow.

We observe less of a clear trend in u_g^*, shown in Fig. 6 as a function of Θ. Values of u_g^* are unstable below the onset of net bedload transport [32], so the scatter in the data at small Θ need not be over-interpreted. Even at Shields numbers above onset, however, the trends are less clear than they are for $\langle u_g \rangle$ or B. Nevertheless, gross behavior can be identified. u_g^* is in general smaller for grains moving on top of beds exposed to flows with subcritical Shields numbers in the direction of conditioning, and larger for grains moving on top of conditioned beds in the opposite direction. Although this behavior is consistent with the measurements of $\langle u_g \rangle$, its physical origin is less clear. We would expect that the typical velocity of mobilized grains would be set by the fluid flow [7]. The bulk flow, however, is both independent of the stress history of the bed and is the same regardless of which direction we drive it in our symmetric apparatus. It may be that the grains are responding

to subtle but systematic changes in the surface structure of the bed that are unresolvable by our measurement techniques, and that the changes in u_g^* are due to different collisions with the bed. This interpretation is consistent with the appearance of a trend in u_g^* with the duration of conditioning: u_g^* is larger for longer durations of conditioning flow, where we might expect a smoother bed. Previous observations of a reduction in bed roughness by flows delivering subcritical stresses [25, 26] support this suggestion. However, it is unclear why we see a dependence of u_g^* on the conditioning time but not B or $\langle u_g \rangle$.

IV. DISCUSSION AND CONCLUSIONS

By studying the onset of net sediment transport in granular beds both with and without prior exposure to a conditioning shear flow delivering subcritical bed stress, we found, consistent with previous work, that pre-stressing the bed leads to a strengthening effect such that the onset of motion occurs at higher stresses. However, we also showed that this bed conditioning also caused the bed to be significantly weaker than a freshly settled bed when driven in the direction opposite that of the original conditioning flow. Trends in the fraction of grains that are mobilized largely tracked the behavior of the mean grain velocity, suggesting (consistently with our previous work [7, 32]) that increases in sediment flux near the onset of motion are primarily due to more rather than faster moving grains. However, we also found that the typical speed of moving grains was also different, although much more variable, in the three sets of scenarios tested. Additionally, we also found that the mean grain velocity and fraction of moving grains was insensitive to the duration of the conditioning flow, but that the typical speed of moving grains show a systematic increase with duration.

Previous experiments on the threshold of motion in beds with a stress history have suggested that it is modified largely due to smoothing of the bed [22, 25] due to the removal or settling of protruding grains [26], which may also result in bed compaction [22]. Our observation that bed strengthening is accompanied by a weakening against oppositely directed flows suggests that this simple picture is incomplete, since simple smoothing of the bed should be isotropic. The directionality of the strengthening effect implies that the contacts of the surface grains must themselves be different in different directions. This symmetry breaking could occur by, for example preferential loading of some contacts relative to others (perhaps

connected to subsurface force chains), or could simply be spatially biased to lie preferentially on the front half of surface grains, effectively wedging them into place but not supporting them from behind. Characterizing these possibilities is a task well suited to grain-resolving numerical simulation, where the contacts and associated forces can all be measured. Such simulations may also be able to identify a suitable nondimensional parameter to capture the aspects of the granular microstructure that are needed to predict the critical Shields number, and so extend the classical Shields diagram from a curve in a two-dimensional space spanned by the Shields and Reynolds numbers to a manifold in a higher-dimensional space.

The lack of dependence of the mean grain velocity and the fraction of moving grains on the duration of bed conditioning is more difficult to interpret, particularly because we do see evidence of duration dependence for the typical velocity of moving grains. This latter quantity may be more dependent on the detailed microstructure of the bed than more averaged quantities such as $\langle u_g \rangle$, since moving grains in bedload transport are almost always in contact with the bed surface. Thus, any smoothing of the bed that occurs on long time scales [22, 25, 26] is likely to affect u_g^*. The lack of observable duration dependence for $\langle u_g \rangle$ and B, however, suggests that, at least for those parameters, our conditioning times are asymptotically long. It is unclear how best to evaluate this hypothesis, because the relevant time scale to compare to is not clear [36]. Thus, understanding the time scales of the mechanisms that lead to bed strengthening would also be a valuable question to address in future work.

We close by highlighting some of the implications of our results. Because we find that bed strengthening when driven in one direction is accompanied by a weakening against flows in other directions, erosion rates for systems that experience typical driving in one direction but sporadic driving in other directions may be significantly underpredicted. This situation is likely in, for example, many coastal systems that experience occasional strong storms that come from directions different from their typical driving. Our results also suggest that when the mobilization of sediments is desirable, such as in flushing reservoirs, the directionality of the mobilizing flow is an important consideration, particularly since the stress required to maintain bedload transport may be lower than that that required to initiate it [37].

ACKNOWLEDGMENTS

This research was sponsored by the Army Research Laboratory and was accomplished under Grant Number W911NF-17-1-0164 (M.G., C.S.O., and N.T.O.) The views and conclusions contained in this document are those of the authors and should not be interpreted as representing the official policies, either expressed or implied, of the Army Research Laboratory or the U.S. Government. We also acknowledge support from the National Science Foundation under Grant Number CBET-2002797 (M.D.S.).

---

[1] D. J. Jerolmack and K. E. Daniels, Viewing Earth's surface as a soft-matter landscape, Nat. Rev. Phys. **1**, 716 (2019).

[2] M. Houssais and D. J. Jerolmack, Toward a unifying constitutive relation for sediment transport across environments, Geomorphology **277**, 251 (2017).

[3] J. M. Buffington and D. R. Montgomery, A systematic analysis of eight decades of incipient motion studies, with special reference to gravel-bedded rivers, Water Resour. Res. **33**, 1993 (1997).

[4] S. Dey, Sediment threshold, Appl. Math. Model. **23**, 399 (1999).

[5] T. Pähtz, A. H. Clark, M. Valyrakis, and O. Durán, The physics of sediment transport initiation, cessation, and entrainment across aeolian and fluvial environments, Rev. Geophys. **58**, e2019RG000679 (2020).

[6] M. Houssais, C. P. Ortiz, D. J. Durian, and D. J. Jerolmack, Onset of sediment transport is a continuous transition driven by fluid shear and granular creep, Nat. Commun. **6**, 6527 (2015).

[7] M. Galanis, P. Wang, M. D. Shattuck, C. S. O'Hern, and N. T. Ouellette, Onset of grain motion in eroding subaqueous bimodal granular beds, Phys. Rev. Fluids **6**, 094301 (2021).

[8] L. Vanel, D. Howell, D. Clark, R. P. Behringer, and E. Clément, Memories in sand: Experimental tests of construction history on stress distributions under sandpiles, Phys. Rev. E **60**, R5040 (1999).

[9] A. Drescher and G. de Josselin de Jong, Photoelastic verification of a mechanical model for the flow of a granular material, J. Mech. Phys. Solids **20**, 337 (1972).

[10] H. M. Jaeger, S. R. Nagel, and R. P. Behringer, Granular solids, liquids, and gases, Rev. Mod.

Phys. **68**, 1259 (1996).

[11] T. S. Majmudar and R. P. Behringer, Contact force measurements and stress-induced anisotropy in granular materials, Nature **435**, 1079 (2005).

[12] W. Losert, J.-C. Géminard, S. Nasuno, and J. P. Gollub, Mechanisms for slow strengthening in granular materials, Phys. Rev. E **61**, 4060 (2000).

[13] M. Toiya, J. Stambaugh, and W. Losert, Transient and oscillatory granular shear flow, Phys. Rev. Lett. **93**, 088001 (2004).

[14] B. Utter and R. P. Behringer, Transients in sheared granular matter, Eur. Phys. J. E **14**, 373 (2004).

[15] S. Slotterback, M. Mailman, K. Ronaszegi, M. van Hecke, M. Girvan, and W. Losert, Onset of irreversibility in cyclic shear of granular packings, Phys. Rev. E **85**, 021309 (2012).

[16] Z. A. Benson, A. Peshkov, D. C. Richardson, and W. Losert, Memory in three-dimensional cyclically driven granular material, Phys. Rev. E **103**, 062906 (2021).

[17] B. Gomez, Typology of segregated (armoured/paved) surfaces: some comments, Earth Surf. Process. Landforms **9**, 19 (1984).

[18] F. I. Isla, Overpassing and armouring phenomena on gravel beaches, Mar. Geol. **110**, 369 (1993).

[19] I. Reid, L. E. Frostick, and J. T. Layman, The incidence and nature of bedload transport during flood flows in coarse-grained alluvial channels, Earth Surf. Process. Landforms **10**, 33 (1985).

[20] J. M. Turowski, A. Badoux, and D. Rickenmann, Start and end of bedload transport in gravel-bed streams, Geophys. Res. Lett. **38**, L04401 (2011).

[21] C. C. Masteller, N. J. Finnegan, J. M. Turowski, E. M. Yager, and D. Rickenmann, History-dependent threshold for motion revealed by continuous bedload transport measurements in a steep mountain stream, Geophys. Res. Lett. **46**, 2583 (2019).

[22] D. Paphitis and M. B. Collins, Sand grain threshold, in relation to bed 'stress history': an experimental study, Sedimentology **52**, 827 (2005).

[23] H. Monteith and G. Pender, Flume investigations into the influence of shear stress history on a graded sediment bed, Water Resour. Res. **41**, W12401 (2005).

[24] H. Haynes and G. Pender, Stress history effects on graded bed stability, J. Hydraul. Eng. **133**, 343 (2007).

[25] A.-M. Ockelford and H. Haynes, The impact of stress history on bed structure, Earth Surf. Process. Landforms **38**, 717 (2013).

[26] C. C. Masteller and N. J. Finnegan, Interplay between grain protrusion and sediment entrainment in an experimental flume, J. Geophys. Res. Earth Surf. **122**, 274 (2017).

[27] N. T. Ouellette, H. Xu, and E. Bodenschatz, A quantitative study of three-dimensional Lagrangian particle tracking algorithms, Exp. Fluids **40**, 301 (2006).

[28] N. Mordant, A. M. Crawford, and E. Bodenschatz, Experimental Lagrangian probability density function measurement, Physica D **193**, 245 (2004).

[29] E. Rodríguez-López, P. J. K. Bruce, and O. R. H. Buxton, A robust post-processing method to determine skin friction in turbulent boundary layers from the velocity profile, Exp. Fluids **56**, 6 (2015).

[30] E. Lajeunesse, L. Malverti, and F. Charru, Bed load transport in turbulent flow at the grain scale: Experiments and modeling, J. Geophys. Res. Earth Surf. **115**, F04001 (2010).

[31] M. Houssais and E. Lajeunesse, Bedload transport of a bimodal sediment bed, J. Geophys. Res. Earth Surf. **117**, F04015 (2012).

[32] J. C. Salevan, A. H. Clark, M. D. Shattuck, C. S. O'Hern, and N. T. Ouellette, Determining the onset of hydrodynamic erosion in turbulent flow, Phys. Rev. Fluids **2**, 114302 (2017).

[33] B. Allen and A. Kudrolli, Granular bed consolidation, creep, and armoring under subcritical fluid flow, Phys. Rev. Fluids **3**, 074305 (2018).

[34] J. C. Roseberry, M. W. Schmeeckle, and D. J. Furbish, A probabilistic description of the bed load sediment flux: 2. Particle activity and motions, J. Geophys. Res. Earth Surf. **117**, F03032 (2012).

[35] D. J. Furbish and M. W. Schmeeckle, A probabilistic derivation of the exponential-like distribution of bed load particle velocities, Water Resour. Res. **49**, 1537 (2013).

[36] F. Charru, H. Mouilleron, and O. Eiff, Erosion and deposition of particles on a bed sheared by a viscous flow, J. Fluid Mech. **519**, 55 (2004).

[37] A. H. Clark, M. D. Shattuck, N. T. Ouellette, and C. S. O'Hern, Onset and cessation of motion in hydrodynamically sheared granular beds, Phys. Rev. E **92**, 042202 (2015).